Dynamics of radiationless transitions in large molecular systems: a Franck-Condon-based method accounting for displacements and rotations of all the normal coordinates[*]

Raffaele Borrelli, and Andrea Peluso[*]

Dipartimento di Chimica, Università di Salerno,

I-84081 Baronissi, Salerno, Italy.

e-mail apeluso@unisa.it

July 25, 2003

Abstract

An efficient method to study the dynamics of radiationless transition in large molecular systems is proposed. It is based on the use of the whole set of normal coordinates of vibration and allows for taking properly into account both the displacements and the mix of the normal modes upon transition between two electronic states. The Hamiltonian matrix elements are written in terms of generalized Franck-Condon integrals and are analytically evaluated by recursion formulae. Applications to the $S_2 \rightarrow S_1$ internal conversion in pyrazine and to long range electron transfer between quinones in photosynthetic reaction centres are given.

---

[*]This paper is dedicated to Prof. Attilio Immirzi on the occasion of his 65th birthday.

1

Introduction

Radiationless transitions between electronic states are of paramount importance in chemistry; they affect the emission spectra of almost all chemicals, Kasha's rule,[1] and control the rate of electron transfer (ET) and photochemical reactions.[2,3] Beyond those well known cases, the model of two crossing electronic states has been applied to a variety of thermal reactions, giving, in some cases, better mechanistic insights, being able to clarify what are the chemical factors which determine the shape of the potential energy surfaces (PES) of reacting systems and therefore the heights of reaction barriers, a key point for understanding reactivity.[4,5] Furthermore, even reactions which are known to occur on a single electronic state, such as proton transfers, can be formally treated as radiationless transition between two strongly interacting electronic states.[6,7] The Empirical Valence Bond (EVB) model lies on this idea and represents one of the most general method for deriving analytical expressions of the potential energy surfaces for reacting systems.[6,8,9]

It is therefore of great interest to develop simple strategies and computational tools for treating radiationless transitions in chemical systems with crossing electronic levels. Methods based on the semiclassical approximation,[10,11] and on Tully's surface hopping model,[12,13] have been widely used, for example see ref 14 and references therein, but in some cases the disagreement with the full quantum mechanical results can be significant.[15,16] Several general methods have been described in the literature for full quantum dynamical calculations,[17–19] they have been applied to non-radiative electronic transitions with very promising results,[19,20] but their applications to large molecular systems remain limited to a few cases.[21–23]

In this paper we intend to give a contribution in this direction by developing a simple and reliable approach tailored for the study of electronic transitions, in which all vibrational degrees of freedom are taken into account in the calculation of the quantum evolution operator. The inclusion in the dynamics of the whole set of vibrational coordinates as active modes, *i.e.* modes whose quantum number changes during the transition, is not possible and perhaps also unuseful, but, as will be shown here, there are no computational difficulties in building up the evolution

operator making use of the whole set of vibrational coordinates of the system and that should lead to a more realistic approach to molecular dynamics.

One of the problem to be faced with when all vibrational degrees of freedom are taken into account is the very large number of parameters to be considered, *i.e.* at least the whole matrix of harmonic force constants, whose reliability can be sometime questionable, posing further problem toward understanding. The somewhat unusual approach proposed here allows to formulate the Hamiltonian operator in terms of molecular properties which can be obtained by experimental data, such as equilibrium geometries and vibrational frequencies of the initial and final PESs, thus providing a more direct link between the parameters to be used in dynamics and experimental data. That is done in a convenient way by using the normal coordinates of each electronic states and by expressing the coupling elements in terms of Franck-Condon integrals. The approach appears to be particularly suitable for all those cases where the initial and final states can be both isolated as stationary states as, for instance, in long range ET in supramolecular assemblies, where one of the two redox sites can be often selectively removed, allowing for a complete characterization of both electronic states and is also very useful for interpreting spectral properties.

In the next sections we will be briefly summarize how the Hamiltonian matrix is built up. Then we will test the performance of the approach with a suitable test case, the $S_2 \rightarrow S_1$ radiationless transition in pyrazine. We will finally discuss an application to the analysis of the mechanism of long range electron transfer between the primary and the secondary quinone in photosynthetic reaction centres, showing that the application of molecular dynamic simulations to relevant biological process can provide important insights for understanding the mechanism of fast biological processes, see ref 24 for a recent review.

Calculation of the Hamiltonian matrix

Let us consider a molecular system characterized by two or more electronic states, which become close in energy in a region of nuclear coordinates, so that a transition

between them can occur.

As is well known, the Born-Oppenheimer approximation breaks down in this case[25–27] and a correlated treatment of electronic and nuclear motion is required. This is accomplished by expanding the time dependent vibronic wavefunction over a set of Born-Oppenheimer product functions:

$$\Psi_{tot}(q, Q, t) = \sum_{l,\bar{v}} c_{l\bar{v}}(t)|l(q, Q)\rangle|\bar{v}_l(Q)\rangle = \sum_{l,\bar{v}} c_{l\bar{v}}(t)|l\bar{v}_l\rangle, \qquad (1)$$

where the subscript l labels the electronic state, $\bar{v}_l$ indicates the whole set of vibrational quantum numbers, $i.e.$ $|\bar{v}_l\rangle = |v_{l1}, v_{l2}, ..v_{ln}\rangle$, n is the number of vibrational degree of freedom, and q and Q denote the electron and nuclear coordinates, respectively. That expansion is always possible because the $|l\bar{v}_l\rangle$'s form a complete set.

On the assumption that there are L electronic states well separated in energy from all the others, the above expansion can be limited to these electronic states and the total Hamiltonian can be written as:

$$\mathcal{H} = \sum_{l,m}^{L} |l\rangle\mathcal{H}_{lm}\langle m|, \qquad (2)$$

where:

$$\mathcal{H}_{lm} = \langle l|\mathcal{T}_N + \mathcal{H}_{el}|m\rangle, \qquad (3)$$

$\mathcal{T}_N$ being the nuclear kinetic energy operator and $\mathcal{H}_{el}$ the total electronic Hamiltonian.

The electronic states to be used in the expansion of the total time-dependent wavefunction can be indifferently adiabatic, $i.e.$ eigenstates of the electronic Hamiltonian, or diabatic states, $i.e.$ states which are smooth functions of the nuclear coordinates. The expansion coefficients of 1 can be determined by solving the time dependent Schrödinger equation:

$$
-i\hbar
\begin{pmatrix}
\dot{\mathbf{C}}_{1\bar{v}}(t) \\
\dot{\mathbf{C}}_{2\bar{w}}(t) \\
. \\
. \\
\dot{\mathbf{C}}_{L\bar{z}}(t)
\end{pmatrix}
=
\begin{pmatrix}
\mathbf{H}_{11} & \mathbf{H}_{12} & . & . & \mathbf{H}_{1L} \\
\mathbf{H}_{12}^{\dagger} & \mathbf{H}_{22} & . & . & \mathbf{H}_{2L} \\
 & & . & . & . \\
 & & . & . & . \\
\mathbf{H}_{1L}^{\dagger} & \mathbf{H}_{2L}^{\dagger} & . & . & \mathbf{H}_{LL}
\end{pmatrix}
\begin{pmatrix}
\mathbf{C}_{1\bar{v}} \\
\mathbf{C}_{2\bar{w}} \\
. \\
. \\
\mathbf{C}_{L\bar{z}}
\end{pmatrix},
\tag{4}
$$

with the appropriate initial conditions, see for instance ref 28.

Throughout this paper, we will freeze rotations and assume harmonic approximation for vibrational motions; that allows to retain a certain simplicity in the formulae without affecting generality. The inclusion of anharmonic effects is straightforward and will be shortly discussed afterwards.

We use the vibrational eigenstates of $\mathcal{H}_{ll}$, $|\bar{v}(Q_l)\rangle$, as basis functions for the expansion 1; with that choice, the $\mathbf{H}_{ll}$'s of eqn 4 are diagonal matrices whose elements are given by:

$$
\langle \bar{w}|\mathcal{H}_{ll}|\bar{v}\rangle = \delta_{\bar{w},\bar{v}} \sum_{i=1}^{n} (v_i + 1/2)\hbar\omega_{li},
\tag{5}
$$

where ω_{li} is the harmonic frequency of the i-th normal mode of the system in the electronic state $|l\rangle$ and the summation runs over all the normal modes of the system; the orthogonality of both adiabatic and diabatic electronic wavefunctions have been used.

As concerns the coupling terms, if $|l\rangle$'s are chosen as eigenstates of the electronic Hamiltonian, $\langle l|\mathcal{H}_{el}|m\rangle = \delta_{lm}E_l^{el}$ and therefore only kinetic couplings have to be considered, whereas in the case $|l\rangle$'s are diabatic states, the electronic coupling term predominates, so that kinetic couplings, although different from zero,[29] can usually be neglected. In some cases it is a good approximation to consider $\mathcal{H}_{lm}$ as a constant. In fact, if the coupling is weak, $\langle l\bar{w}|\mathcal{H}|m\bar{v}\rangle$ will be different from zero only in a small region of the nuclear coordinates where the two electronic states cross each other, so that the Q-dependence of $\mathcal{H}_{lm}$ can be safely neglected and the coupling matrix elements are simply the Franck-Condon (FC) integrals, *i.e.* the overlap between the vibrational states of $|l\rangle$ and $|m\rangle$, times a constant factor:

$$\langle \bar{w} | \mathcal{H}_{lm} | \bar{v} \rangle = const \cdot \langle \bar{w} | \bar{v} \rangle. \tag{6}$$

On the other hand, when the coupling term is large, its dependence upon the vibrational coordinates cannot be neglected. $\mathcal{H}_{lm}$ is usually a function of a subset of normal modes, often referred to as *promoting* modes. It is immaterial to express $\mathcal{H}_{lm}$ in terms of the normal modes of $|l\rangle$, $\mathbf{Q}_l$, or of $|m\rangle$, $\mathbf{Q}_m$, since the two sets of normal coordinates, although different each other because the two electronic states have different equilibrium geometries and different curvatures at the equilibrium points, are related by the affine Duschinsky's transformation:[30]

$$\mathbf{Q}_l = \mathbf{J}\mathbf{Q}_m + \mathbf{K}, \tag{7}$$

where $\mathbf{J}$ is a rotation matrix and $\mathbf{K}$ a displacement vector.

In the case $|l\rangle$ and $|m\rangle$ are chosen as adiabatic electronic states, the only coupling term is provided by the nuclear kinetic energy operator:

$$\mathcal{H}_{lm}(Q_w) = -\frac{\hbar^2}{2} \sum_k \left(\langle l | \frac{\partial}{\partial Q_{wk}} | m \rangle \frac{\partial}{\partial Q_{wk}} + \langle l | \frac{\partial^2}{\partial Q_{wk}^2} | m \rangle \right) + c.c., \qquad w = l, \ or \ m. \tag{8}$$

The terms in the second derivative of the electronic wavefunction usually play a minor role and for most purposes can be neglected. The terms in the first derivative show a dependence over the normal coordinates which can be expressed as a sum of Lorentzian functions,[31,32] each of them can be well approximated by a Gaussian function. In the latter case, the coupling term along the k-th mode will be given by a sum of terms of the form:

$$b e^{-\alpha(Q_{wk}-Q_{wk}^0)^2} \frac{\partial}{\partial Q_{wk}} \qquad w = l, or \ m, \tag{9}$$

where α and b are the width and the height of the Gaussian function centered at $\{Q_{wk}^0\}$, along the k-th mode.

In the case the functional form of $\mathcal{H}_{lm}(Q)$ is not known, a Taylor expansion is

used:

$$\mathcal{H}_{lm}(Q_w) = \text{const} + \sum_k \left(\beta_k Q_{wk} + \frac{1}{2} \sum_j \beta_{kj} Q_{wk} Q_{wj} + ... \right) \qquad (10)$$

By using the recursion relations of harmonic oscillator wavefunctions, it can be easily shown that both in the case of eqn. 10 and of eqn. 9 analytical expressions of $\mathbf{H}_{12}$ can be given in terms of Franck-Condon integrals, see appendix. Thus, the computation of the coupling blocks of the Hamiltonian matrix of eq. 4 requires only an efficient method to evaluate the Franck-Condon integrals. There are several procedures in the literature;[27,33–36] for the sake of completeness the formulae used in this work, their generalization for including kinetic coupling in the form of eq.n 9, and the main points of the derivation, are summarized in the appendix.

A test case: the photophysics of pyrazine

The photophysics of pyrazine is a well suited problem for testing the performance of the approach outlined above. Indeed, that problem has attracted considerable interest over the past years and therefore experimental and theoretical data are abundant in the literature.[37–47]

The absorption spectrum of pyrazine exhibits a well structured band for the $S_0 \to S_1(\pi, \pi^*)$ transition and a broad, less structured band for the $S_0 \to S_2(n, \pi^*)$ one.[37,38] The most significant feature of the S_1 absorption band is the presence of an anharmonic progression of the b_{1g} mode (ν_{10a}); since the molecular symmetry (D_{2h}) is retained upon transition to S_1,[43,46,48] odd transitions of that progression are not allowed in the Franck-Condon approximation (strong frequency variation could be responsible for even transitions), so that other mechanisms must be invoked.

On the basis of the observed isotopic effect on the intensities of the ν_{10a} vibronic bands of the S_1 absorption spectrum, Orlandi and Siebrand ruled out the possibility of a Herzberg-Teller intensity borrowing and suggested that a vibronic coupling between S_1 and S_2 could explain both the observed anharmonic progression and the lack of fine structure in the $S_0 \to S_2(n, \pi^*)$ absorption band;[47] indeed, a fast (30 fs) $S_2 \to S_1$ internal conversion was recently observed by time resolved spectroscopy.[49]

Theoretical computations have confirmed the existence of a conical intersection

between the two excited states,[42] moreover, quantum dynamic computations based on the vibronic coupling mechanism were able to reproduce the shape of the $S_0 \rightarrow S_2$ absorption band.[41,50–52]

In order to apply the procedure outlined in the previous section to the dynamics of the $S_2 \rightarrow S_1$ internal conversion, the equilibrium geometries, the harmonic frequencies and the normal modes of the ground state and of the two crossing excited states are necessary. We will adopt diabatic electronic states, which we assume to be harmonic. Since the two excited diabatic states belong to different irreducible representation, they can only be coupled by a non-displaced mode and therefore the equilibrium geometries of the diabatic states coincide with those of the adiabatic ones. Thus, those parameters, and, as a first approximation, vibrational frequencies and normal modes of vibration have been computed at MCSCF level, see *infra* for details. All results are summarized in table 1 and table 2.

<center>INSERT TABLE 1</center>

<center>INSERT TABLE 2</center>

As concerns the coupling between S_2 and S_1, in D_{2h} point group Q_{10a} is the only mode with the right symmetry (b_{1g}) for linearly coupling S_2 and S_1, thus, following previous work[39,41,50] we have taken a linear expansion over Q_{10a}:

$$\mathcal{H}_{12} = \beta Q_{10a}; \tag{11}$$

the expansion coefficient β (1.3 eV/Å) has been determined by the $S_0 \rightarrow S_1$ progression of the $10a$ mode.

From the minimum energy geometries of table 1 and the relative normal modes, the displacement vectors $\mathbf{K}$ and the rotation matrices $\mathbf{J}$ of eqn. 7 for the $S_0 \rightarrow S_2$, $S_0 \rightarrow S_1$ and $S_2 \rightarrow S_1$ transitions have been build up, eqn.s 21 and 22. In all the electronic transitions only the five a_g modes are displaced, see table 3. The $\mathbf{J}$ rotation matrix relative to the $S_2 \rightarrow S_1$ transition shows a slight Duschinsky coupling for the two b_{3g} modes (ν_3, ν_{8b}), and for the three a_g modes ($\nu_{9a}, \nu_{8a}, \nu_1$). No significant mixings are observed for the $S_0 \rightarrow S_1$ and the $S_0 \rightarrow S_2$ transitions.

<center>8</center>

The Hamiltonian matrix for the $S_2 \rightarrow S_1$ transition have then been build up by using eqn.s 29 and 28.

Since our aim is only to test the reliability of the method, we have performed calculation in which excitations were limited to the 3 a_g modes, ν_1, ν_{6a}, ν_{8a}, and to the active mode, ν_{10a}, keeping the remaining vibrations in their ground state.

The initial wavepacket has been built up by assuming that pyrazine is excited from its ground vibrational state of S_0 by an extremely short light pulse, modelled by a Dirac $\delta(t)$ function. Under this condition the state prepared in the electronically excited state can be described by the first order approximation:

$$|\Psi(0)\rangle = -i\hat{\mu}|S_0\rangle|\bar{0}\rangle, \tag{12}$$

where

$$\hat{\mu} = \sum_{k=1,2,v} |S_k\rangle|\bar{v}\rangle\mu_{0k}\langle\bar{v}|\bar{0}\rangle\langle\bar{0}|\langle S_0|, \tag{13}$$

i.e. by projecting the ground vibrational state of S_0 on the vibrational states of S_1 and S_2.

In order to reproduce the relative intensities of the S_2 and S_1 absorption spectrum the ratio of the transition moments has been taken to be $\mu_{02}/\mu_{01} = 2.5$, which is very close to the experimental one, *ca.* 3.2, obtained from the oscillator strengths of the relative absorption bands.[43]

The time evolution of $|\Psi(0)\rangle$ has been determined by solving the time dependent Schrödinger equation, *cf.* eq. (4), by using the Lanczos algorithm.[53]

Convergence on the computed vibrational frequencies has been obtained by using ten excited states for ν_1, nine for ν_{6a} and ν_{10a} and eight for ν_{8a}, for each electronic state.

The probability that the system, prepared by vertical excitation from S_0 is found in S_2 at time t is shown in figure 1. The population of S_2 rapidly falls off in about 40 fs, in very good agreement with the result of pump-probe photoelectron spectroscopy, 30 fs,[49] and previous quantum dynamical simulations.[20,41]

The fast decay is followed by damped oscillations with low amplitude for about 200 fs, afterwards the probability of S_2 is very close to zero until 1 ps. It is worth of noticing that, also with a limited number of states (*ca.* 20000), an irreversible dynamics, at least in the picosecond time scale, has been obtained.

Once $\Psi(t)$ has been determined, the absorption spectrum can be calculated from the Fourier transform of the autocorrelation function $\langle\Psi(0)|\Psi(t)\rangle$[54]

$$I(\omega) \propto \int_{-\infty}^{+\infty} e^{-t/\tau} e^{-i\omega t} \langle\Psi(0)|\Psi(t)\rangle dt. \tag{14}$$

The exponential function $\exp(-t/\tau)$ is a phenomenological damping factor which accounts for the broadening absorption lines due to spontaneous emission, and for the effects of the dephasing caused by the remaining 20 vibrational modes, whose excitations have not been considered in dynamics. In order to obtain a good Fourier transformation of the autocorrelation function a Hamming apodization function has been used.[55]

In figure 2 the calculated $S_1(n\pi^*)$ absorption spectrum of pyrazine in the gas phase at 0 K is shown, together with the Franck-Condon factors, which, in the absence of vibronic coupling, determine the relative intensities of the absorption peaks. Following previous works a damping factor $\tau = 500$ fs was used to reproduce the linewidth.[50]

The full line spectrum, obtained from eq. 14, shows two peaks at 395 and 903 cm^{-1} which, by comparison with the experimental spectrum, can be assigned to the $10a_0^1$ and $10a_0^2$ transitions. We note that our assignment of the $9a$ and $8a$ modes is inverted with respect to the experimental one,[43,46] thus the experimental $9a_0^1$ peak corresponds to our $8a_0^1$. The $6a$ mode, which is mainly a bending of the angle $\angle$ CNC, shows the most intense progression; the intensities of the progressions of the totally symmetric modes are in good agreement with the experimental ones, indicating

10

that the optimized geometries of the excited and ground electronic states and their normal modes of vibration are reliable. In the calculated spectrum the activity of the mode 1 is more pronounced than in the experimental absorption spectrum. The observed lower activity for that mode has been explained in terms of an anharmonic coupling between the modes 1 and 10a, which is not included in our model.[39] A detailed comparison between the computed and the observed transitions is reported in table 4.

INSERT TABLE 4

In figure 3 the calculated $S_2(\pi\pi^*)$ absorption spectrum is shown, together with the Franck-Condon factors. In this case to reproduce the envelope of the spectrum a damping factor $\tau = 35$ fs was used.[50]

INSERT FIGURE 3

The broad $S_2(\pi\pi^*)$ absorption profile is quite different from the vibrational Franck-Condon structure, showing both variations in peaks positions and intensities. Indeed, the intensities of the $6a_0^1$, $6a_0^2$ and $6a_0^1 1_0^1$ peaks in the spectrum calculated from eq. 14 (full line) differs significantly from the Franck-Condon intensities (bars). In table 5 the computed and observed transition for the main peaks are reported, showing a fairly good agreement.

INSERT TABLE 5

Long range electron transfer in biosystems

Although applicable to any internal conversion, the above approach was originally tailored for studying electron transfer (ET) processes. In fact, in the case of ground state ET most of the input parameters, *i.e.* geometries and vibrational frequencies, can be obtained directly from experiments. Here, we will consider the problem of long range ET between the primary (Q_A) and the secondary quinone (Q_B) in bacterial photosynthetic reaction centres, because, as for pyrazine, this biochemical system has been well characterized both as concerns the three-dimensional

11

structure,[56–58] as well as the thermodynamics and the kinetics of ET.[59–64] We will draw attention only to the internal dynamics of the two cofactors leading to ET, thus considering only an isolated, solvent free, supermolecule constituted by the two redox cofactors and the interposed bridge. The spatial arrangement found in the X-ray structure of *Rhodobacter sphaeroides* frozen under illumination,[58] shown in figure 4, has been adopted.[65] According to current theories for long range ET, in that spatial arrangement ET from Q_A^- to Q_B should promptly occur by tunnelling or superexchange mechanisms, for an alternative point of view see ref.s 66–68.

<center>INSERT FIGURE 4</center>

In the case of through space tunnelling, we assume that there are only two low lying diabatic electronic states, with the unpaired electron fully localized either on Q_A ($|A\rangle$) or Q_B ($|B\rangle$). The total Hamiltonian operator is therefore:

$$\mathcal{H} = |A\rangle[T_N + U_A]\langle A| + |B\rangle[T_N + U_B]\langle B| +$$
$$|A\rangle\mathcal{H}_{AB}\langle B| + c.c. \tag{15}$$

We will adopt harmonic approximation, both because the energy difference between the two electronic states is small and because normal mode displacements are also small, see infra, so that highly excited vibrational states are not expected to be involved in the dynamics. Since the two quinones are far apart each other, we can safely assume that in the diabatic states the potential energy of the system can be written as the the sum of two terms, one for each quinone. U_A and U_B are therefore given by:

$$U_A = \frac{1}{2}(\bar{\mathbf{q}}_1^\dagger \bar{\boldsymbol{\omega}}_1^2 \bar{\mathbf{q}}_1 + \mathbf{q}_2^\dagger \boldsymbol{\omega}_2^2 \mathbf{q}_2), \tag{16}$$

$$U_B = \frac{1}{2}(\mathbf{q}_1^\dagger \boldsymbol{\omega}_1^2 \mathbf{q}_1 + \bar{\mathbf{q}}_2^\dagger \bar{\boldsymbol{\omega}}_2^2 \bar{\mathbf{q}}_2) + \Delta E_{AB}, \tag{17}$$

where $\boldsymbol{\omega}_1$ and $\boldsymbol{\omega}_2$ are the diagonal matrices of the vibrational frequencies, $\mathbf{q}_1$ and $\mathbf{q}_2$ the normal mode vectors of Q_A and Q_B, the bar indicates vibrational coordinates

<center>12</center>

and frequencies of the semiquinone anion and ΔE_{AB} is the energy difference between $|A\rangle$ and $|B\rangle$.

The minimum energy geometries, the vibrational frequencies and the normal modes of vibration of quinones and semiquinone anions have been computed at DFT/B3LYP level of computations; p-benzoquinones (pBQ) have been used as model for the *in vivo* ubiquinones. From the two sets of optimized geometries and the relative normal modes, the rotation matrix $\mathbf{J}$ and the displacement vector $\mathbf{K}$ have been determined and, from them, the active modes for ET have been identified. The rotation matrix and the displacement vector are reported in table 6 together with the computed harmonic frequencies. There are 6 displaced modes, of course all belonging to the a_g irreducible representation of D$_{2h}$ point group, and 12 mixed modes. Among the a_g modes only that at 454 cm^{-1} is significantly displaced, (0.47 Å(a.m.u.)$^{\frac{1}{2}}$). That mode is expected to play the major role in ET dynamics, both because FC integrals between vibrational states differing for one or more quanta on this mode will be larger and because its frequency (0.056 eV) is comparable to the energy gap between ET reactants and products (0.07 eV).[63] As concerns Duschinsky effect, there are 12 modes which are only slightly mixed each other, *cf.* table 3, but most of them fall in the region of higher frequencies, whereas those at lower frequency are so slightly mixed that their role in the dynamics is not expected to be important in the case under examination.

INSERT TABLE 6

For ΔE_{AB} the experimental Gibb's free energy change for ET from Q_A^- to Q_B in *Rhodobacter sphaeroides*, –0.07 eV,[63] will be adopted.

As concerns the electronic coupling operator, we will neglect its dependence over the nuclear coordinates because the normal mode displacements are small and therefore ET dynamics will take place only in a small region of the potential energy surfaces of $|A\rangle$ and $|B\rangle$, in which the electronic coupling element can be considered independent from the nuclear coordinates. With that assumption $\mathcal{H}_{AB}$ becomes a multiplicative factor whose value can be obtained either from empirical expressions relating the exponential fall off of $\mathcal{H}_{AB}$ with the distance between the two redox

sites, or from *ab-initio* computations, using the most suited nuclear configurations. From Hopfield's expression:[69]

$$\mathcal{H}_{AB} = \frac{2.7}{\sqrt{N_a N_b}} \ \exp(-0.72R) \qquad \text{in eV,} \qquad (18)$$

where R (Å) is the edge-to-edge distance between the two aromatic groups a and b of N_a and N_b atoms, $\mathcal{H}_{AB}$=0.85 cm^{-1} is obtained by keeping R=13.1 Å, the shortest (O-O) distance, and using 1/2 as normalization factor (molecular orbital computations suggest that the unpaired electron is mainly localized on the two quinone oxygens, rather than on the whole cycle). The above value is significantly lower than that obtained by *ab initio* MRCI computations, 17 cm^{-1}, obtained as one-half of the energy difference between the first two doublet states of a model system, consisting of two benzoquinone H-bonded to two imidazole rings each of them coordinated to a Zn-acetate, optimized under C_2 symmetry.[70] Since ET from Q_A to Q_B occurs in a time scale much slower than the nuclear relaxation one, we will assume that ET takes place from the ground vibrational level of $|A\rangle$ or from a Boltzmann weighted distribution.

Preliminary computations performed by exciting all the displaced modes each at a time have shown that the most important contribution to ET dynamics comes from the excited vibrational states of the lowest frequency displaced modes, mixed modes and high frequency displaced modes playing really no role in ET. We have thus included in ET dynamics excited vibrational states of the two lowest frequency modes, whose role can be important for filling up the energy gap between reactants and products, and of the three lowest frequency displaced mode of both quinone and semiquinone; thus ten modes are allowed to be excited in dynamics, giving rise to 1048000 vibrational states, and, more important, the Hamiltonian matrix is built up by considering all the sixty modes of the two quinones.

ET probabilities as function of time, obtained by setting $\mathcal{H}_{AB}$=1, from Hopfield's expression, and $\mathcal{H}_{AB}$=20 cm^{-1}, from *ab initio* MRCI computations, are reported in figure 5. ET probabilities have been computed taking as initial state the ground vibrational state of the system, since several tests have shown that the choice of

the initial state as a Boltzmann distribution of vibrational states of Q_A^- does not significantly affect dynamics.

Transition probabilities are very low, the maximum probabilities is $2.5 \cdot 10^{-3}$ in about 130 fs, in contrast with the fact that, *in vivo*, ET occurs with high efficiency, close to unity. In order to get high transition probabilities, the electronic coupling element must be increased of two order of magnitudes (with $\mathcal{H}_{AB}$=550 cm^{-1} the maximum transition probability is 0.63), but such a value appears to be unreasonably high. Alternatively, the energy difference must be decreased; in fact, according to Marcus' theory ET via tunnelling occurs after the initial and final states have reached a nuclear configuration for which the two potential energy surfaces cross each other.[71] By setting ΔE_{AB}=0.0, the transition probability rises to unity, but transition times are significantly longer, 6 ps for $\mathcal{H}_{AB}$=20 cm^{-1} and 120 ps for $\mathcal{H}_{AB}$=1 cm^{-1}, *cf.* figure 6. However, if the resonance condition is slightly perturbed, ΔE_{AB}=10 cm^{-1}, ET probability falls off below 0.08 in the case of $\mathcal{H}_{AB}$=20 cm^{-1} and $2 \cdot 10^{-4}$ for $\mathcal{H}_{AB}$=1, as shown in figure 7.

The above results show that ET via tunnelling requires a very stringent energy condition, which could not be fulfilled in the particular case under study. In fact ET between quinones in bacterial photosynthetic reaction centres involves only the lowest energy vibrational states of the two quinones, both because the process is slow enough for Q_A^- relaxes in its ground vibrational states or in a Boltzmann weighted distribution of vibrational states and because of the small energy difference between the initial and final states. In such a small energy interval the Franck-Condon weighted density of states is expected to be small and therefore the hypothesis that a continuum of final states weakly coupled to the initial state, assuring that the degeneracy condition is fulfilled, is highly questionable.

15

Our results are in line with the previous finding that tunnelling is not an efficient mechanism for ET in those cases where the distance between the two redox sites is longer than 8 Å,[69] and that alternative mechanisms could be operative in systems with much longer site separations.[66]

Conclusion

The novelty of the present approach to the dynamics of radiationless transitions consists of using the normal coordinates of vibration of each electronic state in the computation of the Hamiltonian matrix governing the temporal evolution of quantum systems. With that choice, the key parameters controlling the dynamics are, apart of course the electronic coupling terms, the displacements of the equilibrium positions and the mixing of the normal modes upon transition, so that a more direct link between dynamics and molecular properties is established, with a significant benefit in understanding. The analysis of the displacement vector ($\mathbf{K}$) and of the rotation matrix ($\mathbf{J}$) allows for selecting the active modes, *i.e.* those modes whose quantum number will change upon transition. It is known from a long time that the most displaced modes play a predominant role in radiationless transitions,[71] but it has been recently recognized that also the mixing of the normal coordinates can play a significant role;[10,72,73] our approach takes automatically both effects into account.

Another important aspect of the above approach is that, even though a limited set of active modes is used in dynamics, the effect of all other vibrational coordinates is taken into account in the calculation of the Hamiltonian matrix elements. That is a crucial point for determining realistic values of vibronic couplings, the crucial parameters in dynamics. The importance of including the whole set of vibrational coordinates in the theoretical analysis of the absorption spectrum of pyrazine has already pointed out by Raab et al.[20] and therefore we will not further comment that case. As concerns ET between quinones in photosynthetic reaction centres, we have found that the inclusion of all modes is relevant. For a quantitative estimate, it is sufficient to specify that when all modes are taken into account the effective coupling between the two vibrational ground state is about one third than that obtained by

considering the most displaced mode. Thus, as previously mentioned, modes which seem to have little effect on the temporal evolution of a molecular system, either because their equilibrium positions are only slightly displaced or because they are slightly mixed for the effect of the transition, see table 6, can significantly affect the time evolution of a molecular system when considered all together.

Anharmonic effects can be easily taken into account by using a polynomial expansion in terms of the normal modes of each electronic state;[74] integrals containing third or fourth order terms in the expansion of the potential energy can be analytically computed by using the recursion formulae for Hermite polynomials.[75]

Finally, it is worth of noticing that most of the required input parameters, *i.e.* the vibrational frequencies and the normal modes of each electronic states involved in dynamics can be now reliably obtained from the most common packages for electronic structure calculations, without any modification, so that the procedure proposed here can be easily interfaced with such programs.

It is our opinion that the approach presented in this paper is flexible and can be used for the analysis of several chemical processes (for an application to problems involving three electronic states see ref. 70). The main practical limit of the above procedure is in the number of FC integrals which can be stored in the computer memory, since the direct computation of Franck-Condon integrals (as for two electron integrals in SCF computations) is not recommended with the analytical integrals of the appendix. That problem can be partially solved by using the binary tree approach developed by Gruner[76] and recently improved by Ruhoff,[77] which should significantly reduce the amount of memory needed to store the FC integrals and the time needed for their calculation. Work aimed to find out a faster way to calculate the Franck-Condon integrals for direct implementation is in progress.

Computational details

The equilibrium geometries and the vibrational frequencies of the ground electronic state, and of the S_1 and the S_2 electronic states of pyrazine have been optimized at CASSCF level using the standard cc-pVDZ basis set. The active space

includes six π orbitals (three occupied and three unoccupied) and two occupied non-bonding orbitals of the nitrogens. Vibrational frequencies have been computed at the optimized geometries with analytical energy derivative.

The minimum energy geometries, the vibrational frequencies and the normal modes of vibration of quinones and semiquinone anions have been computed at DFT/B3LYP level of computations with the standard 6-31++G** basis set; MCSCF and DFT computations have been performed by the Gaussian 94 package.[78]

For the computation of the electronic coupling element for direct tunnelling, we have first fully optimized the structure of figure 4 at ROHF/3-21G level of the theory imposing C_2 symmetry and then performed a MRCI computation using the MC basis set for Zn and the 6-31G one for all other atoms. The active space employed in CI includes 11 molecular orbitals, of which four doubly and one singly occupied, whereas the external space consisted of the lowest 10 virtual orbitals not included in the active space. Only single and double excitations have been considered for building up the reference space, whereas only singly excited determinants obtained by promoting electrons from the reference to the external space have been included in CI computations. The GAMESS program has been used for all CI computations.[79]

Franck-Condon factors have been computed by the FCDYN package (available on request).[80]

18

Appendix: Evaluation of Franck-Condon integrals

The two sets of normal modes $\mathbf{Q}_1$, and $\mathbf{Q}_2$ differ because the two electronic states have different equilibrium geometries and different curvatures at the equilibrium points. However, they are related by the affine transformation proposed by Duschinsky[30]

$$\mathbf{Q}_1 = \mathbf{J}\mathbf{Q}_2 + \mathbf{K}, \tag{19}$$

where $\mathbf{J}$ is a rotation matrix and $\mathbf{K}$ a displacement vector.

If the normal modes of the two electronic states are expressed in terms of Cartesian coordinates $\boldsymbol{\xi}$ of the nuclei, which greatly simplify the treatment with respect to internal coordinates,[36,81] the following equations can be written:

$$\boldsymbol{\xi} - \boldsymbol{\xi}_1^0 = \mathbf{L}_1\mathbf{Q}_1 \qquad \boldsymbol{\xi} - \boldsymbol{\xi}_2^0 = \mathbf{L}_2\mathbf{Q}_2 \tag{20}$$

where $\boldsymbol{\xi}_1^0$ and $\boldsymbol{\xi}_2^0$ are the equilibrium nuclear coordinates of the electronic states $|1\rangle$ and $|2\rangle$ respectively, and $\mathbf{L}_1$ and $\mathbf{L}_2$ are the rectangular matrices of the normal modes of the two electronic states.

In this case the rotation matrix and the displacement vector of equation 19 are given by:

$$\mathbf{J} = \mathbf{L}_1^\dagger \mathbf{S}\mathbf{L}_2 \tag{21}$$

$$\mathbf{K} = \mathbf{L}_1^\dagger(\mathbf{S}\boldsymbol{\xi}_2^0 - \boldsymbol{\xi}_1^0) \tag{22}$$

The matrix $\mathbf{S}$ accounts for the so called zero-order axis-switching effects in the normal mode transformation.[82,83]

Indicating with $\mathbf{A}$ the diagonal matrix of the amplitudes α_s of the Gaussian coupling of eq. 9 and with the vector $\bar{\mathbf{Q}} = \{Q_{lk}^0\}$ the center of the Gaussian then the expression for the FC integral between ground vibrational states is:

$$\langle\bar{0}|\bar{0}\rangle = (\det\boldsymbol{\Gamma}_1 \det\boldsymbol{\Gamma}_2)^{1/4}\left(\frac{2^N \det\mathbf{J}}{\det\mathbf{X}}\right)^{1/2}\exp\left(-\mathbf{Z}_1 + \frac{1}{2}\mathbf{Y}_3^\dagger\mathbf{X}^{-1}\mathbf{Y}_3\right), \tag{23}$$

where:

$$\boldsymbol{\Gamma}_i = \boldsymbol{\omega}_i/\hbar; \quad i = 1, 2, \tag{24}$$

$$\mathbf{Z}_1 = \bar{\mathbf{Q}}^\dagger \mathbf{A} \bar{\mathbf{Q}} + \frac{1}{2}\mathbf{K}^\dagger \mathbf{\Gamma}_1 \mathbf{K}, \tag{25}$$

$$\mathbf{Y}_3^\dagger = 2\bar{\mathbf{Q}}^\dagger \mathbf{A} - \mathbf{K}^\dagger \mathbf{\Gamma}_1 \mathbf{J} \tag{26}$$

$$\mathbf{X} = \mathbf{J}^\dagger \mathbf{\Gamma}_1 \mathbf{J} + \mathbf{\Gamma}_2 + 2\mathbf{A}, \tag{27}$$

and the recurrence relations which allow to compute any FC integral are:

$$
\begin{aligned}
v_\mu \langle \bar{v} | \bar{w} \rangle = {}& [v_\mu(v_\mu - 1)]^{1/2}(P_{\mu\mu} - 1)\langle v_1...v_\mu - 2...v_n | \bar{w} \rangle \\
&+ \sum_{i \neq \mu}(v_\mu v_i)^{1/2} P_{\mu i}\langle v_1...v_i - 1...v_\mu - 1...v_n | \bar{w} \rangle \\
&+ \sum_i (v_\mu w_i)^{1/2} R_{\mu i}\langle v_1...v_\mu - 1...v_n | w_1...w_i - 1...w_n \rangle \} \\
&+ \left(\frac{v_\mu}{2}\right)^{1/2} T_\mu\langle v_1...v_\mu - 1...v_n | \bar{w} \rangle.
\end{aligned}
\tag{28}
$$

$$
\begin{aligned}
w_\mu \langle \bar{v} | \bar{w} \rangle = {}& [w_\mu(w_\mu - 1)]^{1/2}(P'_{\mu\mu} - 1)\langle \bar{v} | w_1...w_\mu - 2...w_n \rangle \\
&+ \sum_{i \neq \mu}(w_\mu w_i)^{1/2} P'_{\mu i}\langle \bar{v} | w_1...w_i - 1...w_\mu - 1...w_n \rangle \\
&+ \sum_i (v_i w_\mu)^{1/2} R_{i\mu} \langle v_1...v_i - 1...v_n | w_1...w_\mu - 1...w_n \rangle \\
&+ \left(\frac{w_\mu}{2}\right)^{1/2} T'_\mu\langle \bar{v} | w_1...w_\mu - 1...w_n \rangle.
\end{aligned}
\tag{29}
$$

where the matrices $\mathbf{P}, \mathbf{P}', \mathbf{R}, \mathbf{T}, \mathbf{T}'$ are given by

$$
\begin{aligned}
\mathbf{P} &= 2\mathbf{\Gamma}_1^{1/2}\mathbf{J}\mathbf{X}^{-1}\mathbf{J}^\dagger\mathbf{\Gamma}_1^{1/2}; \qquad \mathbf{P}' = 2\mathbf{\Gamma}_2^{1/2}\mathbf{X}^{-1}\mathbf{\Gamma}_2^{1/2} \\
\mathbf{T} &= 2\mathbf{K}^\dagger\mathbf{\Gamma}_1^{1/2} + 2\mathbf{Y}_3^\dagger\mathbf{X}^{-1}\mathbf{J}^\dagger\mathbf{\Gamma}_1^{1/2}; \qquad \mathbf{T}' = 2\mathbf{Y}_3^\dagger\mathbf{X}^{-1}\mathbf{\Gamma}_2^{1/2} \\
\mathbf{R} &= 2\mathbf{\Gamma}_1^{1/2}\mathbf{J}\mathbf{X}^{-1}\mathbf{\Gamma}_2^{1/2}
\end{aligned}
\tag{30}
$$

Using this recurrence relations the full Hamiltonian matrix can be generated in an efficient way.

References and Notes

1. Kasha, M. *Discussion Faraday Soc.* **1950,** *9,* 14.

2. Pross, A.; Shaik, S. S. *Acc. Chem. Res.* **1983,** *16,* 363.

3. Bixon, M.; Jortner, J. *J. Chem. Phys.* **1968,** *48,* 715.

4. Shaik, S. S. *J. Am. Chem. Soc.* **1981,** *103,* 3692.

5. Pross, A. *Acc. Chem. Res.* **1985,** *18,* 212.

6. Chang, Y. T.; Miller, W. H. *J. Phys. Chem.* **1990,** *94,* 5884.

7. Sagnella, D. E.; Tuckerman, M. E. *J. Chem. Phys.* **1998,** *108,* 2073.

8. Warshel, A.; Weiss, R. M. *J. Am. Chem. Soc.* **1980,** *102,* 6218.

9. Warshel, A. *Acc. Chem. Res.* **1981,** *14,* 284.

10. Heller, E. *Acc. Chem. Res.* **1981,** *14,* 368.

11. Miller, W. H. *J. Phys. Chem. A* **2001,** *105,* 2942.

12. Tully, J. C.; Preston, R. K. *J. Chem. Phys.* **1971,** *55,* 562.

13. Tully, J. C. In *Modern Methods for Multidimensional Dynamics Computations in Chemistry;* World Scientific: Singapore, 1998.

14. a) Heller, E. J.; Davis, M. J. *J. Phys. Chem.* **1982,** *86,* 2218 surface hopping in transizioni non radiative. b) Warshel, A.; Stern, P. S.; Mukamel, S. *J. Chem. Phys.* **1983,** *78,* 7498. c) Warshel, A.; Chu, Z. T.; Parsom, W. W. *Science* **1989,** *246,* 112.

15. Volobuev, Y. L.; Hack, M. D.; Truhlar, D. G. *J. Phys. Chem. A* **1999,** *103,* 6225.

16. Ferretti, A.; Granucci, G.; Lami, A.; Persico, M.; G., V. *J. Chem. Phys.* **1996,** *104,* 5517.

17. Wyatt, R.; Zhang, J. Z. H. *Dynamics of Molecules and Chemical Reactions;* Dekker: New York, 1996.

18. Trahan, C. J.; Hughes, K.; Wyatt, R. E. *J. Chem. Phys.* **2003,** *118,* 9911.

19. Beck, M. H.; Jäckle, A.; Worth, G. A.; Meyer, H.-D. *Phys. Rep.* **2000,** *324,* 1.

20. Raab, A.; Worth, G. A.; Meyer, H.-D.; Cederbaum, L. S. *J. Chem. Phys.* **1999,** *110,* 936.

21. Stuchebrukhov, A. A.; Marcus, R. A. *J. Chem. Phys.* **1993,** *98,* 6044.

22. Hammerich, A. D.; Manthe, U.; Kosloff, R.; Meyer, H.-D. *J. Chem. Phys.* **1994,** *101,* 5831.

23. Fang, J.-Y.; Guo, H. *Chem. Phys. Lett.* **1995,** *235,* 341.

24. Warshel, A. *Acc. Chem. Res.* **2002,** *35,* 385-395.

25. Born, M.; Oppenheimer, R. *Ann. Phys. (Paris)* **1927,** *84,* 457.

26. Herzberg, G.; C., L.-H. H. *Disc. Faraday Soc* **1963,** *35,* 77.

27. Peluso, A.; F., S.; Del Re, G. *Int. J. Quantum Chem.* **1997,** *63,* 233.

28. a) Feynman, R. P. *The Feynman Lecture on Physics: Volume 3;* Addison-Wesley, Pub. Co: Massachussets, 1966. b) Del Re, G.; Förner, W.; Hofmann, D.; Ladik, J. *Chem. Phys.* **1989,** *139,* 265. c) Bixon, M.; Jortner, J. *Adv. Chem. Phys* **1999,** *106,* 35. d) Warshel, A.; Parson, W. W. *Ann. Rev. Phys. Chem.* **1991,** *42,* 279.

29. Mead, C. A.; Truhlar, D. G. *J. Chem. Phys.* **1979,** *70,* 2284.

30. Duschinsky, F. *Acta Phisicochim. URSS* **1937,** *7,* 551.

31. Desouter-Lecomte, M.; Ley-Nihant, B.; Praet, M. T.; Lorquet, J. C. *J. Chem. Phys.* **1987,** *86,* 1429.

32. Desouter-Lecomte, M.; Lorquet, J. C.; Van Pires, M. *J. Chem. Phys.* **1979,** *71,* 3661.

33. Doktorov, E. V.; Malkin, I. A.; I., M. V. *J. Mol. Spec.* **1975,** *56,* 1.

34. Sharp, T. E.; Rosenstock, K. M. *J. Chem. Phys.* **1964,** *41,* 3453.

35. Kupcka, H.; Holbrich, G. *J. Chem. Phys.* **1985,** *55,* 3975.

36. Warshel, A.; Karplus, M. *Chem. Phys. Lett.* **1972,** *17,* 7.

37. Suzuka, I.; Mikami, N.; Ito., M. *J. Mol. Spec.* **1974,** *52,* 21.

38. Suzuka, I.; Udagawa, Y.; Ito, M. *Chem. Phys. Lett.* **1979,** *64,* 333.

39. Heider, N.; Fischer, S. F. *Chem. Phys.* **1984,** *88,* 209.

40. Seidner, L.; Stock, G.; Sobolewski, A. L.; Domcke, W. *J. Chem. Phys.* **1992,** *96,* 5298.

41. Schneider, R.; Domcke, W. *Chem. Phys. Lett.* **1988,** *150,* 235.

42. Woywod, C.; Domcke, W.; Sobolewski, A. L.; Werner, H.-J. *J. Chem. Phys.* **1994,** *100,* 1400.

43. Innes, K. K.; Ross, I. G.; Moomaw, W. R. *J. Mol. Spectrosc.* **1988,** *132,* 492.

44. Innes, K. K.; Simmons, J. D.; Tilford, S. G. *J. Mol. Spectrosc.* **1963,** *11,* 257.

45. Innes, K. K.; Byrne, J.; Ross, I. G. *J. Mol. Spectrosc.* **1967,** *22,* 125.

46. McDonald, D. B.; Rice, S. A. *J. Chem. Phys.* **1981,** *74,* 4893.

47. Orlandi, G.; Siebrand, W. *J. Chem. Phys.* **1973,** *58,* 4513.

48. Zalewski, E. F.; McClure, D. S.; Narva, D. L. *J. Chem. Phys.* **1974,** *61,* 2964.

49. Stert, V.; Farmanara, P.; Radloff, W. *J. Chem. Phys.* **2000,** *112,* 4460.

50. Stock, G.; Domcke, W. *J. Phys. Chem.* **1993,** *97,* 12466.

51. Schneider, R.; Domcke, W.; Köppel, H. *J. Chem. Phys.* **1990,** *92,* 1045.

52. Wolfseder, B.; Domcke, W. *Chem. Phys. Lett.* **1995,** *235,* 370.

53. Park, J. T.; Light, J. C. *J. Chem. Phys.* **1986,** *85,* 5870.

54. Gordon, R. C. Adv. Magn. Res.. In , Vol. 3; 1968.

55. Ernst, R. R.; Bodenhausen, G.; Wokaun, A. *Principles of Nuclear Magnetic Resonance in One and Two Dimensions;* Claredon Press: Oxford, 1981.

56. Deisenhofer, J.; Epp, O.; Miki, K.; Huber, R.; Michel, H. *Nature* **1985,** *318,* 618.

57. Deisenhofer, J.; Michel, H. *EMBO J.* **1989,** *8,* 2149.

58. Stowell, M. H. B.; McPhillips, T.; Rees, D. C.; Soltis, S. M.; Abresch, E.; Feher, G. *Science* **1997,** *276,* 812.

59. Vos, M. H.; Lambry, J.; Robles, S. J.; Youvan, D. C.; Breton, J. *Proc. Natl. Acad. Sci. USA* **1992,** *89,* 613.

60. Lin, S.; Taguchi, A. K. W.; Woodbury, N. W. *J. Phys. Chem.* **1996,** *100,* 17067.

61. Woodbury, W. T.; Parson, W. W. *Biochi. Biophys. Acta* **1984,** *767,* 345.

62. Gunner, M. R.; Dutton, L. P. *J. Am. Chem. Soc.* **1989,** *111,* 3400.

63. Kleinfeld, D.; Okamura, M. Y.; Feher, G. *Biochemistry* **1984,** *23,* 5780.

64. Kleinfeld, D.; Okamura, M. Y.; Feher, G. *Biochim. Biophys. Acta* **1985,** *809,* 291.

65. Brookhaven Protein Data Bank.

66. Peluso, A.; Di Donato, M.; Saracino, G. A. A. *J. Chem. Phys.* **2000,** *113,* 3212.

67. Peluso, A.; Di Donato, M.; Saracino, G. A. A.; Improta, R. *J. Theor. Biol.* **2000,** *207,* 101.

68. Peluso, A.; Brahimi, M.; Carotenuto, M.; Del Re, G. *J. Phys. Chem. A* **1998,** *102,* 10333.

69. Hopfield, J. J. *Proc. Natl. Acad. Sci. USA* **1974,** *71,* 3640.

70. Peluso, A.; Di Donato, M.; Villani, G., submitted for publication.

71. Marcus, R. A. *J. Chem. Phys.* **1956,** *24,* 979.

72. Sando, G. M.; Spears, K. G. *J. Phys. Chem. A* **2001,** *105,* 5326.

73. Kotelnikov, A. I.; Medvedev, E. S.; Medvedev, D. M.; Stuchebrukhov, A. A. *J. Phys. Chem. B* **2001,** *105,* 5789.

74. Califano, S.; Adembri, G.; Sbrana, G. *Spectrochim. Acta* **1964,** *20,* 385.

75. Wilson, E. B. J.; Decius, J. C.; Cross, P. C. *Molecular vibrations;* Dover Publications: New York, 1980.

76. Gruner, D.; P., B. *Chem. Phys. Lett.* **1987,** *138,* 310.

77. Ruhoff, P. T.; Ratner, M. A. *Int. J. Quantum Chem.* **2000,** *77,* 383.

78. Frisch, M. J.; Trucks, G. W.; Schlegel, H. B.; Gill, P. W.; Johnson, B. G.; Robb, M. A.; Cheeseman, J. R.and Keith, T.; Petersson, G. A.; Montgomery, J. A.; Raghavachari, K.; Al-Laham, M. A.; Zakrzewski, V. G.; Ortiz, J. V.; Foresman, J. B.; J., C.; B., S. B.; Nanayakkara, A.; Challacombe, M.; Peng, C. Y.; Ayala, P. Y.; W., C.; W., W. M.; S., A. J. L. R. E.; Gomperts, R.; Martin, R. L.; Fox, D. J.; Binkley, J. S.; Defrees, D. J.; Baker, J.; Stewart, J. P.; Head-Gordon, M.; Gonzales, C.; Pople, J. A. *Gaussian 94, Revision C.2;* Gaussian Inc.: Pittsburgh PA, 1995.

79. Schmidt, M. W.; Baldridge, K. K.; Boats, J.; Elbert, S. T.; Gordon, M. S.; Jensen, J. J.; Koseki, S.; Matsunaga, M.; Nguyen, K. A.; Su, S.; Windus, T. L.; Dupuis, M.; Montgomery, J. A. *J. Comput. Chem.* **1993,** *14,* 1347.

80. `http://pcdual.chem.unisa.it` .

81. Warshel, A. *J. Chem. Phys.* **1975,** *62,* 214.

82. Watson, J. K. G. *Mol. Phys.* **1968,** *15,* 479.

83. Houghen, J. T.; Watson, J. K. G. *Can. J. Phys.* **1965,** *43,* 298.

Table 1: Equilibrium geometries (Å, deg) of the ^1A_g (S_0), $^1B_{3u}$ (S_1), and $^1B_{2u}$ (S_2) states of Pyrazine, and relative energies, calculated at CASSCF level.

parameter	^1A_g $E = 0$	$^1B_{3u}$ $E = 4.95(3.94)^a$	$^1B_{2u}$ $E = 5.94(4.84)^a$
r(CN)	1.332	1.356	1.371
r(CC)	1.396	1.385	1.432
r(CH)	1.082	1.079	1.081
∠ CNC	115.74	119.12	111.76
∠ CCN	122.13	120.44	124.12
∠ HCN	117.14	119.37	116.63

a) Reference 38.

.

Table 2: Vibrational Frequencies (cm^{-1}) of the ^1A_g, $^1B_{3u}$ (S$_1$) and $^1B_{2u}$ (S$_2$) states of pyrazine computed at CASSCF level, cc-pVDZ basis set.

| vibration | | ^1A_g | | $^1B_{3u}$ | | $^1B_{2u}$ |
Notation[a]	Irrep[b]	CASSCF	exptl[c]	CASSCF	exptl[d]	CASSCF
6a	a_g	641	596	643	585	645
1	a_g	1082	1015	1042	970	976
9a[e]	a_g	1743	1582	1723	1377	1628
8a[e]	a_g	1319	1230	1284	1104	1266
2	a_g	3367	3055	3396		3383
12	b_{1u}	1113	1021	1085		1170
19a[e]	b_{1u}	1225	1416	1152		1083
18a[e]	b_{1u}	1623	1139	1573		1566
13	b_{1u}	3343	3012	3373		3363
14	b_{2u}	1087	1149	973		737
15	b_{2u}	1528	1063	1519		1463
19b	b_{2u}	1151	1416	1171		1071
20b	b_{2u}	3361	3036	3391		3378
6b	b_{3g}	758	704	746	662	735
3	b_{3g}	1455	1346	1410		1389
8b	b_{3g}	1669	1525	1584		1519
7b	b_{3g}	3341	3040	3370		3361
16a	a_u	406	341	398	400	454
17a	a_u	999	960	978	743	966
10a	b_{1g}	955	919	930	383	915
4	b_{2g}	781	756	786	552	791
5	b_{2g}	993	983	978	518	958
16b	b_{3u}	455	420	493	236	512
11	b_{3u}	831	785	797		816

a) Reference 46. b) Irreducible representation. c) Reference 43 d) Reference 46. e) Assignment different from ref 43 and ref 46.

Table 3: Mass weighted displacements of a_g normal modes of pyrazine.

vibration	$K(^1A_g - ^1B_{3u})$	$K(^1A_g - ^1B_{2u})$	$K(^1B_{3u} - ^1B_{2u})$
6a	0.278	-0.324	0.587
1	-0.123	0.286	0.196
9a	0.140	0.066	0.129
8a	0.009	0.038	0.011
2	-0.018	-0.009	0.006

Table 4: Computed and observed transitions and their relative intensities of the $S_0 \rightarrow S_1$ absorption spectrum of pyrazine.

Assignment	Shift cm^{-1}		Relative Intensity	
	Computed	Observed[a]	Computed	Observed[a]
0-0	-	-	100	100
$6a_0^1$	635	583	48	80
$6a_0^2 + 8a_0^1$	1295	1172	48	44[b]
$10a_0^1$	395	383	22	17
$10a_0^2$	903	826	36	16
1_0^1	1045	970	26	3[c]

a) From ref. 46. b) In our calculations the transitions $6a_0^2$ and $8a_0^1$ are exactly degenerate, hence the intensity value 44 refers to the sum of the two experimental intensities. c) See the text for the difference between the observed and calculated intensity.

Table 5: Computed and observed transitions and their relative intensities of the $S_0 \rightarrow S_2$ absorption spectrum of pyrazine.

Assignment	Shift cm^{-1}		Relative Intensity	
	Computed	Observed[a]	Computed	Observed[a]
0-0	-	-	70	67
1_0^1	1060	958	100	100
1_0^2	1964	1889	76	90
$6a_0^1 1a_0^1$	1652	1552	63	86

a) From ref. 38.

Table 6: Frequencies (cm^{-1}), displacements (Åamu$^{\frac{1}{2}}$) and mixing coefficients of the normal modes of pBQ and pBQ^{-}.

Mode	ω pBQ	pBQ^{-}	$\Delta\omega$	**K**	**J** $\bar{q} = $ **J** q
$1b_{3u}$	93.545	129.255	35.710	0.001	
$1b_{2g}$	222.364	308.631	86.267	0.000	
$1a_{u}$	336.187	395.068	58.881	0.000	
$1b_{2u}$	411.499	389.082	-22.417	0.000	
$1a_{g}$	454.220	468.121	13.901	-0.473	
$1b_{3g}$	455.618	470.774	15.156	0.000	.98 $1b_{3g}$ -.16 $2b_{3g}$
$2b_{3u}$	513.679	513.847	0.168	0.002	
$2b_{3g}$	601.156	630.286	29.130	0.000	.17 $1b_{3g}$ +.98 $2b_{3g}$
$1b_{1u}$	754.538	764.365	9.827	-0.010	
$1b_{1g}$	755.060	789.560	34.500	-0.001	
$2a_{g}$	774.099	821.519	47.420	0.150	
$2b_{1g}$	781.091	736.583	-44.508	0.000	.97 $2b_{1g}$ +.20 $3b_{1g}$
$3b_{3u}$	901.426	850.859	-50.566	-0.001	
$2b_{1u}$	947.869	962.813	14.943	0.000	
$2a_{u}$	1009.591	944.865	-64.726	0.000	
$3b_{1g}$	1010.118	936.341	-73.776	0.000	-.18 $2b_{1g}$ +.98 $3b_{1g}$
$2b_{2u}$	1085.794	1077.671	-8.123	0.000	
$3a_{g}$	1168.916	1155.331	13.586	-0.094	
$3b_{3g}$	1237.067	1264.164	27.097	0.000	.96 $3b_{3g}$ +.26 $4b_{3g}$
$3b_{2u}$	1320.373	1231.884	-88.489	0.000	.95 $1b_{2u}$ -.28 $4b_{2u}$
$3b_{1u}$	1385.696	1370.247	-15.448	0.000	.95 $3b_{1u}$ -.30 $4b_{1u}$
$4b_{3g}$	1397.902	1454.347	-56.446	0.000	-.25 $3b_{3g}$ +.96 $4b_{3g}$
$4a_{g}$	1648.909	1501.946	-146.963	0.000	.85 $4a_{g}$ -.51 $5a_{g}$
$4b_{2u}$	1680.332	1491.066	-189.266	0.004	.28 $1b_{2u}$ +.96 $4b_{2u}$
$4b_{1u}$	1736.041	1538.940	-197.100	0.005	.30 $3b_{1u}$ +.95 $4b_{1u}$
$5a_{g}$	1738.235	1651.182	-87.052	-0.162	.51 $4a_{g}$ +.85 $5a_{g}$
$5b_{1u}$	3196.719	3145.006	-51.713	0.000	
$5b_{3g}$	3197.320	3144.347	-52.972	0.000	
$5b_{2u}$	3213.312	3165.081	-48.231	0.000	
$6a_{g}$	3215.552	3169.881	-45.671	0.009	

Figure 1: Decay curve of the S_2 electronic state population ($P_2(t)$) after initial excitation by an ultrashort laser pulse.

Figure 2: $S_0 \rightarrow S_1$ absorption spectrum. Vertical bars are the Franck-Condon factors calculated without the vibronic coupling. A phenomenological damping factor $\tau = 500$ fs has been used. The position of the 0_0^0 peak has been shifted to match the experimental value 323.87 nm.

Figure 3: $S_0 \rightarrow S_2$ absorption spectrum. A phenomenological damping constant $\tau = 35$ fs has been used. The position of the 0_0^0 peak has been shifted to match the experimental value 263.88 nm.

Figure 4: Primary and secondary quinones of photosynthetic reaction centres and the interposed bridge.

Figure 5: ET transition probabilities as a function of time ($\Delta E = 0.07$ eV) a) $V = 1$ cm^{-1} b) $V = 20$ cm^{-1}. In figure a) the ET probability has very small negative values due to the numerical precision of the Lanczos propagation scheme.[53]

Figure 6: As fig. 5 but for $\Delta E = 0$ cm^{-1}

Figure 7: As fig. 5 but for $\Delta E = 10$ cm^{-1}

Figure 1

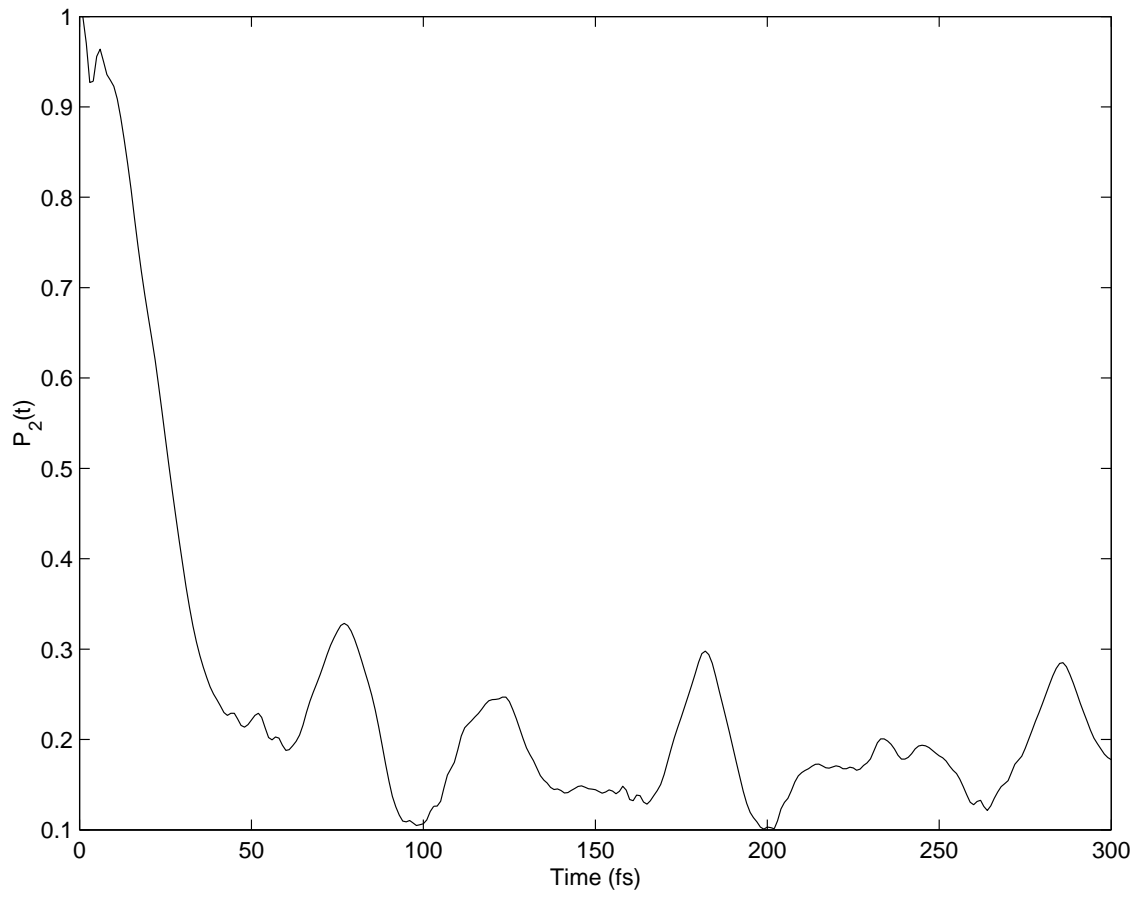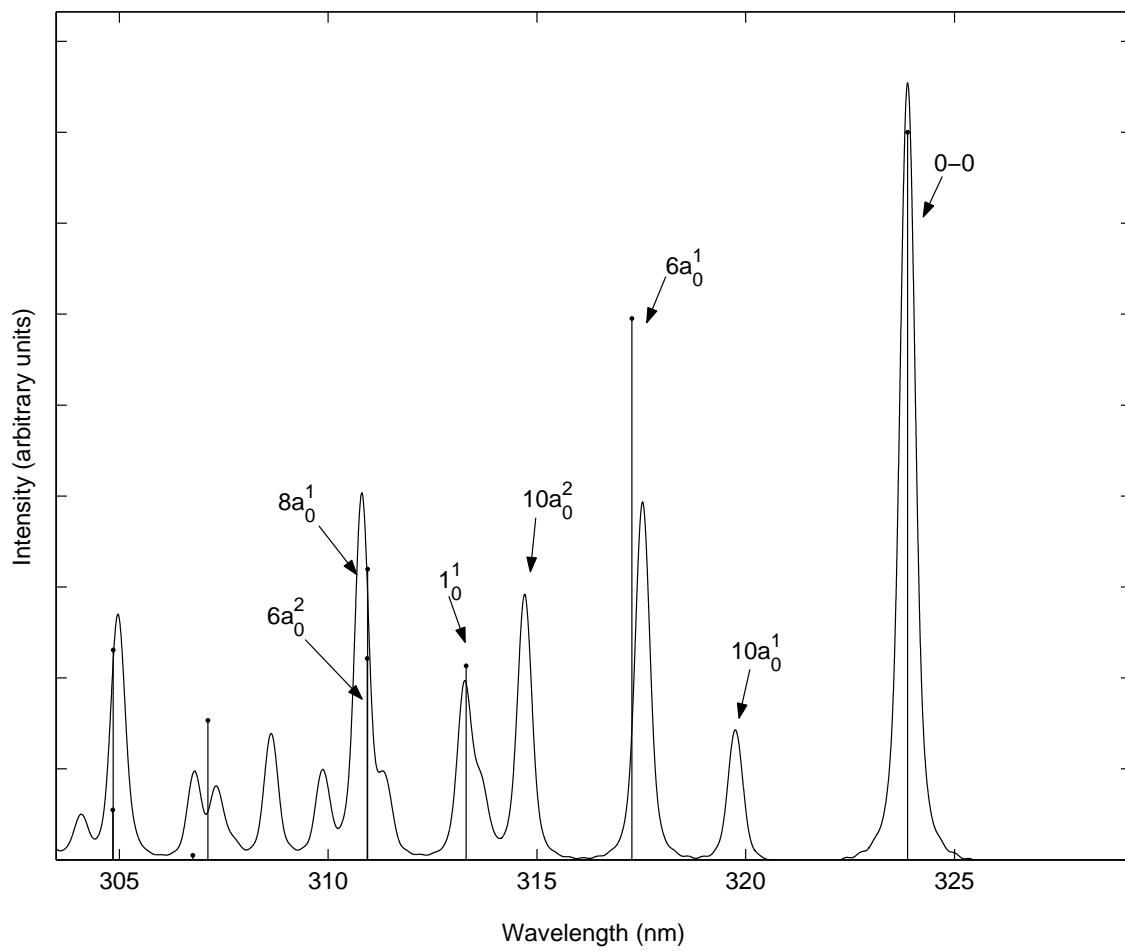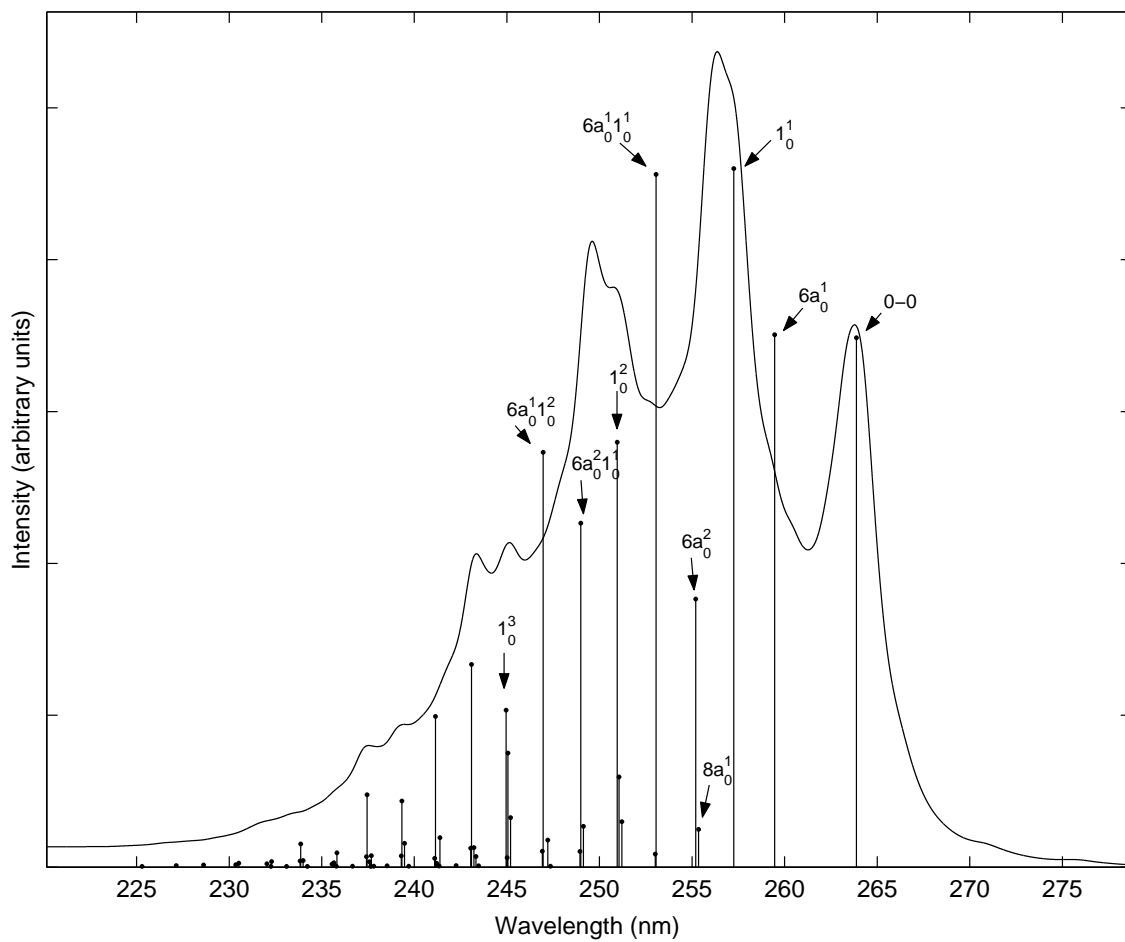**Figure 2**

Figure 3

Figure 4
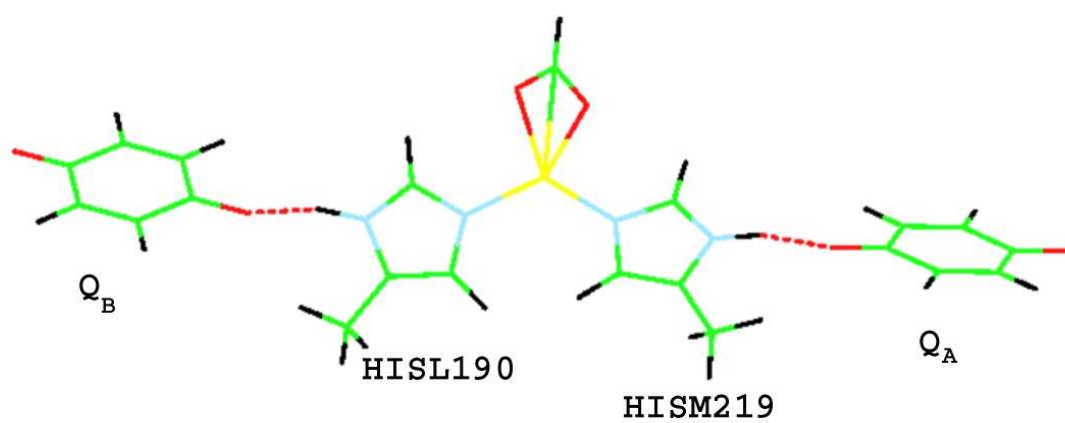
Figure 5

Figure 6

Figure 7